In vitro and *in vivo* evaluation of silk fibroin-hardystonite-gentamicin nanofibrous scaffold for tissue engineering applications

Zhina Hadisi, Hamid Reza Bakhsheshi-Rad, Tavia Walsh, Mohammad Mehdi Dehghan, Saeed Farzad-Mohajeri, Hossein Gholami, … Mohsen Akbari

November 2020

Polymer Testing 91 (2020) 106698

Contents lists available at ScienceDirect

Polymer Testing

journal homepage: http://www.elsevier.com/locate/polytest

In vitro and *in vivo* evaluation of silk fibroin-hardystonite-gentamicin nanofibrous scaffold for tissue engineering applications

Zhina Hadisi [a,b], Hamid Reza Bakhsheshi-Rad [c], Tavia Walsh [a,b], Mohammad Mehdi Dehghan [d,e], Saeed Farzad-Mohajeri [d], Hossein Gholami [d], Anahita Diyanoush [f], Erik Pagan [a,b], Mohsen Akbari [a,b,*]

[a] Laboratory for Innovations in Micro Engineering (LiME), Department of Mechanical Engineering, University of Victoria, Victoria, Canada
[b] Center for Advanced Materials and Related Technologies (CAMTEC), University of Victoria, Victoria, Canada
[c] Advanced Materials Research Center, Department of Materials Engineering, Najafabad Branch, Islamic Azad University, Najafabad, Iran
[d] Institute of Biomedical Research, University of Tehran, Tehran, Iran
[e] Department of Surgery and Radiology, Faculty of Veterinary Medicine, University of Tehran, Tehran, Iran
[f] Department of Polymer Engineering, Amirkabir University of Technology, Tehran, Iran

ARTICLE INFO

Keywords:
Drug delivery
In vivo
Subcutaneous implant
Nanofiber
Electrospinning
Silk fibroin

ABSTRACT

Designing advanced biomaterials with regenerative and drug delivering functionalities remains a challenge in the field of tissue engineering. In this paper we present the design, development, and a use case of an electrospun nano-biocomposite scaffold composed of silk fibroin (SF), hardystonite (HT), and gentamicin (GEN). The fabricated SF nanofiber scaffolds provide mechanical support while HT acts as a bioactive and drug carrier, on which GEN is loaded as an antibacterial agent. Antibacterial zone of inhibition (ZOI) results indicate that the inclusion of 3–6 wt% GEN significantly improves the antibacterial performance of the scaffolds against Gram-negative *Escherichia coli* (*E. coli*) and Gram-positive *Staphylococcus aureus* (*S. aureus*) bacteria, with an initial burst release of 10–20% and 72–85% total release over 7 days. The release rate of stimulatory silicon ions from SF-HT scaffolds reached 94.53±5 ppm after 7 days. Cell studies using osteoblasts show that the addition of HT significantly improved the cytocompatibility of the scaffolds. Angiogenesis, *in vivo* biocompatibility, tissue vascularization, and translatability of the scaffolds were studied via subcutaneous implantation in a rodent model over 4-weeks. When implanted subcutaneously, the GEN-loaded scaffold promoted angiogenesis and collagen formation, which suggests that the scaffold may be highly beneficial for further bone tissue engineering applications.

1. Introduction

Tissue engineering has emerged as a promising approach for addressing the shortages and limitations of available donor organs and tissues in the area of transplantation medicine for bone reconstruction. Various techniques have been proposed to fabricate bone scaffolds including solvent casting [1], salt-leaching [2], freeze-drying [3], sol-gel [4], three-dimensional printing [5], and electrospinning [6]. Among these existing biofabrication methods, electrospinning has been used extensively for bone tissue engineering due to the adaptability in fiber diameter, scaffold pore size, and material properties, enabling adjustments to be made to the biophysical and structural properties of the scaffolds for better recapitulation of multiscale nano- and microstructures of native tissues. Furthermore, electrospinning is easy to use and compatible with a wide range of biomaterials and bioactive molecules [7].

Nanocomposites consisting of organic and inorganic materials have received attention in relation to bone tissue engineering and drug delivery methods due to the nanotopography similarities between nanocomposites and native bone tissue [8]. Nanocomposites are therefore good candidates for bone tissue engineering as they provide a suitable matrix similar to the extra cellular matrix (ECM), desirable cell binding moieties, mechanical stability, and enable controlled drug delivery for bone regeneration [9–12]. Nanocomposites made of bioceramics and biocompatible polymers have been widely used as scaffolding materials for bone tissue engineering [13,14]. A bioceramic is a ceramic material

* Corresponding author. 3800 Finnerty Road, Engineering Office Wing, Victoria, BC, V8P 5C2, Canada.
E-mail address: makbari@uvic.ca (M. Akbari).

https://doi.org/10.1016/j.polymertesting.2020.106698
Received 6 January 2020; Received in revised form 12 June 2020; Accepted 15 June 2020
Available online 6 July 2020

that, when implanted in the body, provides a biological response at the interface of the material, facilitating bond formation between the material and the tissues [13]. Among the available bioceramics, hydroxyapatite (HA, $Ca_5(PO_4)_3(OH)$) is a highly investigated material as it possesses a similar mineral composition to that of bone, in addition to having osteoconductive properties [15,16]. HA-based scaffolds degrade at a very slow rate *in vivo* (up to 24 weeks) however [17], and have poor mechanical properties which prevent complete bone regeneration, thus increasing the risk of bone infections [18]. Calcium silicate ceramics, hardystonite (HT, $Ca_2ZnSi_2O_7$) in particular, have recently gained traction as a new class of biomaterial for bone tissue engineering due to their excellent bioactivity and biodegradability [19]. Several studies have shown that the presence of Zi and Si ions improved bone tissue regeneration, vascularization, and stimulated the differentiation of stem cells into osteogenic cells due to the stimulatory role of zinc and silicon ions present in HT [20,21]. Incorporating HT into polymeric substrates has also shown to significantly improve the mechanical strength of the fabricated scaffolds [22].

Various natural polymers (collagen, chitosan, alginate, chondroitin sulfate, Zein polydopamine, poly (3-hydroxybutyrate-co-2-hydroxyvalerate) (PHBV)) and synthetic polymers (poly (lactic acid) (PLA), poly (caprolactone) (PCL), poly (lactic-coglycolide) (PLGA)) have been studied for bone tissue engineering applications [23–27]. While synthetic polymers have more controllable structures and pose fewer immunological concerns, synthetic polymers have advantages in supporting cell adhesion and function [28]. Among the available biomaterials, silk fibroin (SF) derived from *Bombyx mori* remains a highly promising material for bone tissue engineering due to its excellent biocompatibility, controllable biodegradability, and strong mechanical properties [29]. A recent *in vivo* study evaluated the regeneration efficacy of SF in rats and showed that at 8-weeks post-implantation into calvarial defects, the volume of new bone formation in SF scaffolds was comparable to that of commercial Bio-Gide collagen membranes [30]. Kim et al. have also demonstrated that bone regeneration in a rat calvarial defect is significantly improved when treated with SF scaffolds, when compared to poly lactic acid (PLA) scaffolds [31]. The combination of nanocomposite bioceramics with natural polymers into composite scaffolds which simulate bone ECM have been studied with highly positive results. Gao et al. fabricated such an electrospun gelatin/chitosan/HA scaffold that provided desirable multi-functional characteristics in bone tissue engineering [25].

The poor antibacterial properties of biocomposite scaffolds remain a challenge in tissue engineering, and can lead to severe implant-related bacterial infections and post-surgical complications [32]. According to the American Academy of Orthopedic Surgeons, approximately 33% of the bone implantations lead to infections that end up requiring a second surgery [33]. Systemic antibiotic administration is a common practice used to prevent post-implantation infections, however this approach can result in antibacterial resistance, induced toxicity in vital organs such as the kidneys, liver, and heart, and may negatively affect the patient's gut bacterium [34]. To address these issue, antibiotics can instead be loaded into the scaffolds and delivered locally at the implantation site [35].

In the present study, a biocomposite scaffold is fabricated from electrospun SF nanofibers and functionalized with GEN-loaded HT. A thorough search of the relevant literature did not reveal a previous evaluation of the drug-loading capacity of HT embedded within polymeric nanofiber matrices. The structure and morphology of the electrospun nanofibers was studied using scanning electron microscopy (SEM). The release rate of GEN and ions (Ca^{2+}, Si^{4+}, and Zn^{2+}) from the HT nanofiber component was measured. The antibacterial activity of the GEN-loaded HF-SF scaffolds was evaluated against both Gram-negative (*E. coli*) and Gram-positive (*S. aureus*) bacteria using a disc diffusion and liquid microdilution assay. An *in vitro* biocompatibility analysis of the scaffolds, including cell viability and cell attachment, was performed using osteoblast cells. In a subsequent *in vivo* experiment, the scaffolds were implanted subcutaneously into rats, in order to evaluate *in vivo* biocompatibility, tissue response, and the angiogenic properties of the scaffolds (Fig. 1).

2. Materials

Bombyx mori silk cocoons were provided by the Iranian Silkworm Research Center. SF sponge was extracted from the *Bombyx mori* cocoons following the procedure in a previously published work [36]. HT powder was synthesized via the sol–gel method (Fig. S1). Lithium bromide (LiBr; Sigma-Aldrich, Saint Louis, USA), sodium carbonate (Na_2CO_3; Merck, Germany), cellulose dialysis tube (12 kDa, MWCO, Sigma-Aldrich, Saint Louis, USA), formic acid (98%; Merck, Germany), absolute ethanol (99.7%; Merck, Germany), Gentamicin (Sigma-Aldrich, Saint Louis, USA), 0.01 M phosphate buffered saline tablets (PBS, pH 7.4; Sigma-Aldrich, Saint Louis, USA) and other reagents were of analytical grade.

3. Experimental

3.1. Fabrication and characterization of composite nanofibers

SF sponge was dissolved in formic acid to form a solution of 13 wt%. HT powder of varying concentrations (0, 10, 20, 30, and 40 wt%) were subsequently added to the SF solution and stirred for 24 h at room temperature. GEN of various ratios of HT:GEN (0, 1:0.1, 1:0.3 and 1:0.6) were added to the SF-HT polymer solution and stirred for 2 h at room temperature, prior to electrospinning. The code and composition of each scaffold are summarized in Table S1. An electrospinning apparatus (Fanavaran Nano-Meghyas) was used for fabricating the scaffolds hereafter referred to as SF-HT-xGEN, where x refers to the wt% of loaded GEN. The electrospinning process was performed at room temperature and humidity with a constant flow rate of 0.225 mL/h and a voltage of 10 kV. Scanning electron microscopy (SEM, JEOL JSM-6380LA) was used to evaluate the morphology of the electrospun nanofibers. Image analysis software (Image J) was employed to quantify the diameters of the electrospun nanofibers.

3.2. In vitro study of GEN release from scaffolds

For the *in vitro* study of GEN release from the scaffolds, 100 mg of GEN-loaded scaffolds were immersed in 1 mL of PBS and incubated at 37 °C for 7 days. At each time point, the entirety of the supernatant was collected to determine the cumulative amount of GEN release and replaced with 1 mL of fresh PBS solution. The concentration of released GEN was measured using an ultra-violet spectrophotometer (UV-spec) at a wavelength of 345 nm [37]. The release of Ca^{2+}, Si^{4+}, and Zn^{2+} ions from the HT loaded in the nanocomposite fibers was measured using scaffold samples (2 × 2 cm) were immersed in 1 mL of PBS and incubated at 37 °C for 1 week. At days 3 and 7, 1 mL of supernatant was collected and replaced with fresh PBS solution. The number of released ions was determined using Inductively Coupled Plasma Mass Spectrometry (ICP-MS, Agilent 7500cx).

3.3. Antibacterial test

Gram-negative (*Escherichia coli*, ATCC 9637) and Gram-positive (*Staphylococcus aureus*, ATCC 12600) bacteria were used to assess the antibacterial capabilities of the scaffolds in a disc diffusion antibiotic sensitivity test. The antibacterial effect of scaffolds containing different concentrations of GEN was determined by measuring the area of the ZOI using image analysis software (Image J). The quantitative analysis of the scaffold's antimicrobial performance was based on the liquid medium micro dilution assay, according to a previously published work [38]. The bacterial inhibition percentage was determined using eq. (1), where I_C is defined as the absorbance value of the bacterial suspension control, and I_S is defined as the absorbance value of the bacterial suspension

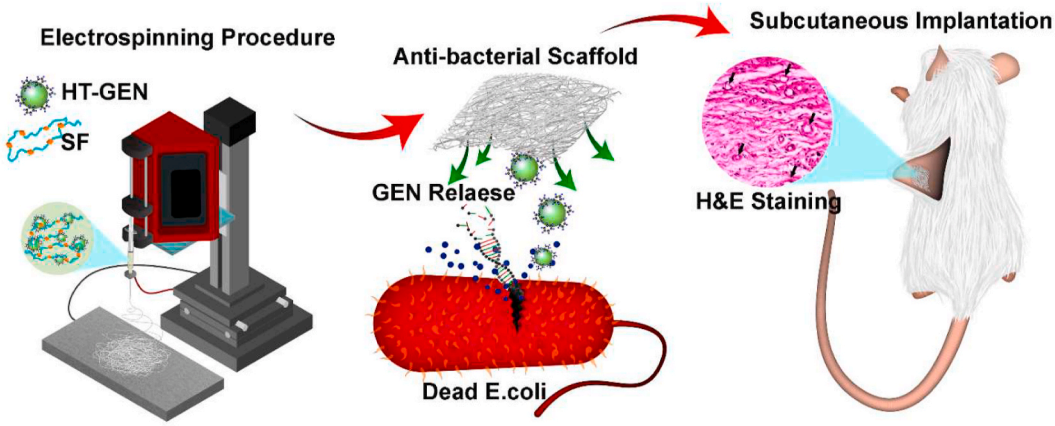

Fig. 1. Schematic illustration of the synthesis of antibacterial SF-HT-xGEN composite scaffolds and subcutaneous implantation in rat model.

containing GEN-loaded scaffolds at each time point.

$$Bacterial\ \ Inhibition\ (\%) = (Ic - Is)/Ic \times 100 \quad (1)$$

3.4. Cell viability study: the extent of cell attachment evaluated on scaffold nanofibers

To assess the extent of cell attachment on the scaffold nanofibers, MG-63 osteoblast cells (Sigma Aldrich, Saint Louis, USA) were seeded onto UV (ultraviolet) sterilized scaffolds at a concentration of 2×10^4 cells/mL and cultured for 3 days. Subsequently, the cell-seeded scaffold constructs were stained with DAPI (4′,6-diamidino-2-phenylindole, blue fluorescence in live cells) and fluorescence image analysis was performed. Scaffold cytocompatibility was assessed using an MTT (3-(4,5-dimethylthiazol-2-yl)-2,5-diphenyltetrazolium bromide) assay to quantify the cell viability. Briefly, MG-63 osteoblast cells were grown in a 48-well plate at a seeding density of 2×10^4 cells/mL and exposed to the scaffolds for 7 days [39]. At days 3 and 7, the absorbance of the formazan solution was measured at 570 nm using a plate reader spectrophotometer.

3.5. Animal study

Fischer rats (150–160 g, 5–6 weeks of age) were housed in sterilized cages with access to sterile food and water. The scaffolds (5 × 2mm) with optimized GEN concentration (as determined by the *in vitro* experiments) were sterilized using UV irradiation. The rats were anaesthetized with 2% isoflurane inhalation and the scaffolds were implanted in the subcutaneous dorsum. After 2- and 4-weeks post implantation, the rats were sacrificed by cervical dislocation, and images of the implanted scaffolds were taken using a digital camera for analysis. The scaffolds were removed for macroscopic imaging and analysis (n = 5 for each time point). All animal protocols were approved by the Institutional Animal Care and Use Committee at the University of Tehran.

3.6. Histopathological staining

Full-thickness wound tissue samples from the two treatment groups were collected and fixed in 10% buffered formalin. Prior to slicing, fixed tissues were transferred to 30% sucrose then sliced into 5 μm-thick frozen sections using a cryostat (Leica Biosystems, Canada). The tissue sections were pre-treated with Bouin Solution (Sigma-Aldrich, Saint Louis, USA) for 15 min at 56 °C, then stained with Hematoxylin and eosin (H&E, Sigma Aldrich, USA).

3.7. Statistical analysis

All experiments were performed in minimum triplicate and presented as Mean ± Standard Deviation. Results were analyzed by GraphPad Prism Version 7 (GraphPad Software, CA, USA). Statistical significance was analyzed using one-way ANOVA and shown by P-value (ns: not significant, $*p < 0.05$).

4. Results and discussion

4.1. Fiber morphology

The SEM images and corresponding fiber size distributions in Fig. 2 show the electrospun SF nanofibers with HT concentrations of 0 wt%, 10 wt%, 20 wt%, 30 wt%, and 40 wt%. The mean electrospun nanofiber diameter was 100 ± 12 nm for nanofibers with 0 wt% HT. The mean diameter increased after HT loading to a maximum observed diameter occurring in 40 wt% HT samples. This diameter increase may be caused by the change in conductivity and viscosity of the electrospinning solution upon the addition of HT. A similar variation in fiber diameter with the addition of osteoinductive materials was found in a study by Zhou et al., where a concentration of HA greater than 40 wt% resulted in the formation of beads and non-continues nanofibers due to the agglomeration of HA particles [40]. As the 40 wt% HT nanofibers resulted in irregular and non-continuous nanofibers (Fig. 2E), the concentration of 30 wt% HT was chosen for the ensuing drug release, *in vitro,* and *in vivo* studies.

4.2. In vitro drug release study

The release profiles of GEN from the composite scaffolds in PBS solution are shown in Fig. 3A, for a time period of 168 h. The obtained results suggest that the release profile had two different phases; an initial burst release followed by a period of sustained release. The initial burst release (10–20%) is attributed to the release of GEN physically adsorbed onto the nanofibers surface, whereas the sustained release was due to the hydrolytic degradation of SF-HT nanofiber scaffold. After 7 days, 72–85% of GEN was released from the SF-HT scaffolds, however the remaining GEN contained within the biocomposite nanofibers may continue to prevent bacterial infection for an extended period of time.

Fig. 3b shows the release of calcium, zinc, and silicon ions from SF-HT scaffolds at days 1, 3 and 7. The ion profile confirmed the gradual release of scaffold degradation byproducts over the 7-day span. The maximum amount of ion release belonged to silicon, which reached 94.53±5 ppm after 1 week of immersion in PBS, whereas the release of both calcium and zinc were observed to be lower. Each of these ions plays an important role in the process of bone regeneration, thus their release from the scaffolds is favorable. Even at low concentrations (10 μM), silicon has been found to stimulate vascularization by upregulating nitric oxide synthase (NOS), resulting in increased vascular endothelial

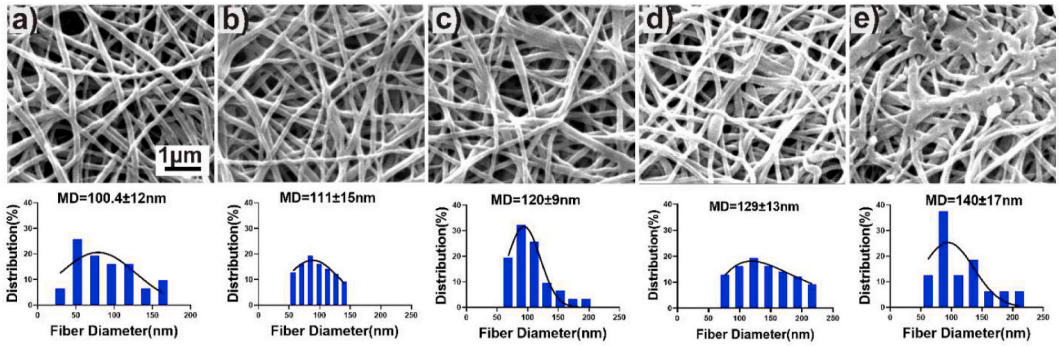

Fig. 2. Characterization of electrospun nanofibers. SEM images and diameter-distribution histograms of (a) SF, (b) SF-10HT, (c) SF-20HT, (d) SF-30HT, and (e) SF-40HT nanofibers (MD = mean diameter).

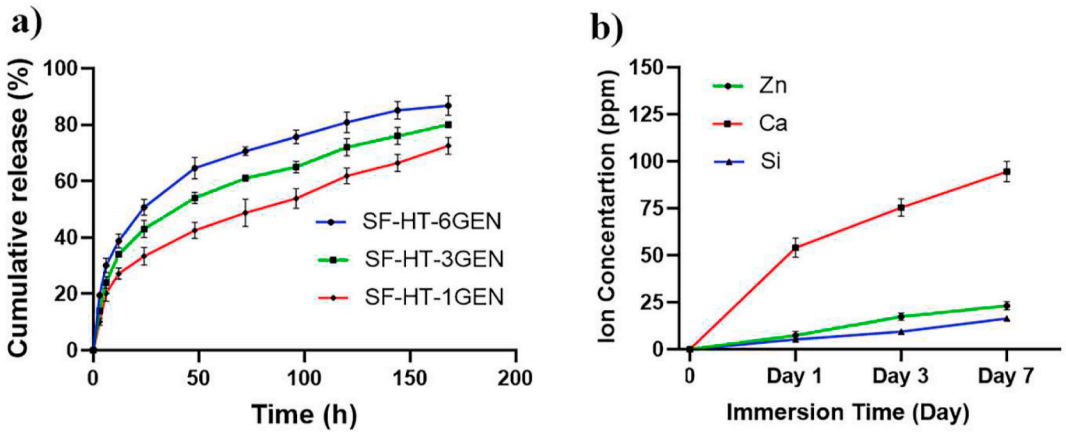

Fig. 3. In vitro release study. (a) Release profile of GEN from composite scaffolds. (b) Ion concentration released from SF-HT scaffolds after immersion in PBS at days 1, 3 and 7.

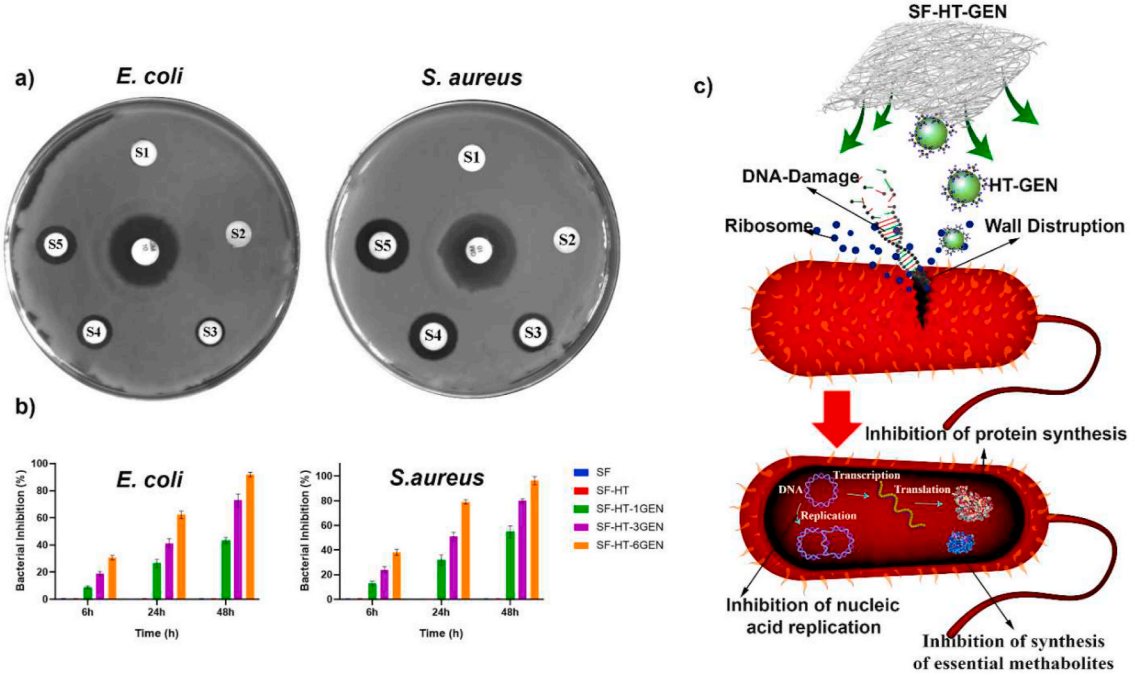

Fig. 4. Antibacterial study. (a) ZOI images of the scaffolds after 24hr against *E. coli* and *S. aureus* (S1 = SF, S2 = SF-HT, S3 = SF-HT-1GEN, S4 = SF-HT-3GEN, and S5 = SF-HT-6GEN). (b) Bacterial inhibition percentage against *E. coli* and *S. aureus* after 6, 24, and 48hr. (c) Illustration of the antibacterial mechanism of SF-HT-xGEN scaffolds.

growth factor (VEGF) generation [41], and has osteogenic differentiation properties [42]. Zinc is particularly involved in the regulation of alkaline phosphatase (ALP) expression, which plays a key role in osteogenesis and mineralization processes, important for the formation of new bone in bone tissue engineering applications [43,44]. Calcium ions are also significant for bone tissue formation, and are mainly involved in bone development through calcification and cellular signaling [45]. Dvorak et al. reported that the optimal calcium concentration for stimulating the proliferation of rat calvarial osteoblasts is 3–10 mM [46].

4.3. Antibacterial activity

Implant-associated infections are one of the most prevalent clinical challenges in medicine. Current preventative strategies rely on the development of antibacterial implants that provide local and sustained drug delivery [47]. GEN, the drug utilized in this study, is a broad-spectrum aminoglycoside antibiotic. Studies have shown that GEN affords a wider antibacterial spectrum against both Gram-negative and Gram-positive bacterium, and has the longest duration of antibacterial activity when compared to other antibiotics such as vancomycin, teicoplanin, ceftazidime, imipenem, piperacillin, and tobramycin [48,49].

The antibacterial activity of SF-HT-xGEN scaffolds against *S. aureus* and *E. coli* was assessed using the disc diffusion method (Fig. 4a). After 24 h of incubation, no inhibition zone was observed around the scaffolds made of plain SF and SF-HT, demonstrating that the base material composition of the electrospun scaffolds do not have inherent antibacterial properties. The addition of GEN in the SF-HT scaffolds significantly increased the size of the inhibition rings for *E. coli,* in the order of SF-HT-6GEN (2.35 ± 0.1 mm) > SF-HT-3GEN (1.22 ± 0.09 mm) > SF-HT-1GEN (0.98 ± 0.1 mm). Similar results were found for *S. aureus* with the addition of GEN; the size of the inhibition ring increased in the order of SF-HT-6GEN (2.87 ± 0.17 mm) > SF-HT-3GEN (1.99 ± 0.09 mm) > SF-HT-1GEN (1.33 ± 0.11 mm). As expected, the bacteria inhibition zone increased with the amount of loaded GEN, confirming the antibacterial activity of the fabricated scaffolds [50]. The enhanced antimicrobial performance of SF-HT-xGEN scaffolds was caused by the diffusion of the GEN from the scaffolds into the agar plate, thus inhibiting bacterial growth. Fig. 4b depicts the percentage of bacterial inhibition for the different scaffold types at incubation times 6, 24, and 48 h. The microdilution assay demonstrated the dose-dependent antimicrobial activity of the SF-HT-xGEN scaffolds. Higher antimicrobial effects were demonstrated on Gram-positive bacteria compared to Gram-negative strains. Fig. 4c demonstrates the mechanism of action of the antibiotic, in which GEN kills bacteria through DNA damage and by inhibiting protein synthesis, nucleic acid replication, and essential metabolite synthesis [50].

4.4. In vitro cell proliferation study

We evaluated the *in vitro* effects of the GEN-loaded scaffold material composition, on the proliferation and attachment of MG-63 osteoblasts. MG-63 is a typical cell line that has been extensively used for *in vitro* toxicity studies [51]. Fluorescent images of the osteoblasts with DAPI staining indicated that the presence of HT in the material increased the cell coverage on the scaffolds (Fig. 5a and b). These results were confirmed by the proliferation assay (Fig. 5f), which showed a significant increase in the metabolic activity of cells grown on scaffolds containing HT. The improvements in cell attachment and proliferation may be attributed to the presence of zinc and silicon in HT, ions which promote the secretion of bone growth factors and protein synthesis [22]. The effect of loaded GEN on cell attachment and proliferation was evaluated, and it was determined that GEN had a non-significant effect on cell attachment and metabolic activity for concentrations up to 3 wt% (Fig. 5c and d). However, increasing the amount of GEN to 6%wt reduced the cell attachment and metabolic activity, which may be due to antibiotic toxicity. Similarly, cellular toxicity has been reported with the incorporation of antibiotics at high dosages, as a result of the stress induced on the cells from disturbed cellular metabolic activity [52,53]. Based on these results, the SF-HT-3GEN scaffold formulation was considered for the subsequent *in vivo* studies.

4.5. In vivo compatibility study for tissue regeneration

In vivo biocompatibility is an important factor to consider for scaffolds used in bone tissue engineering. It is crucial that implanted scaffolds generate a low inflammatory response, promote extracellular matrix deposition, and act as a pro-angiogenic environment. According to the International Standard for biological evaluation of medical devices, the *in vivo* biocompatibility of scaffolds designed for bone and cartilage tissue regeneration should be evaluated through subcutaneous implantation in the hypoderm of a rat [54]. The hypoderm is a highly vascularized tissue with a higher level of metabolism compared to that of bone and cartilage, and is therefore a suitable location for monitoring the angiogenic properties and rapid host inflammatory response to implanted scaffolds [55].

The *in vivo* study proceeded with SF-HT-3GEN scaffolds as opposed to SF-HT-1GEN or SF-HT-6GEN, as the present studies proved that this scaffold exhibited higher antibacterial performance and superior *in vitro* biocompatibility and cytotoxicity. Scaffold biocompatibility, vascularization activity, and cell infiltration were examined with H&E staining of

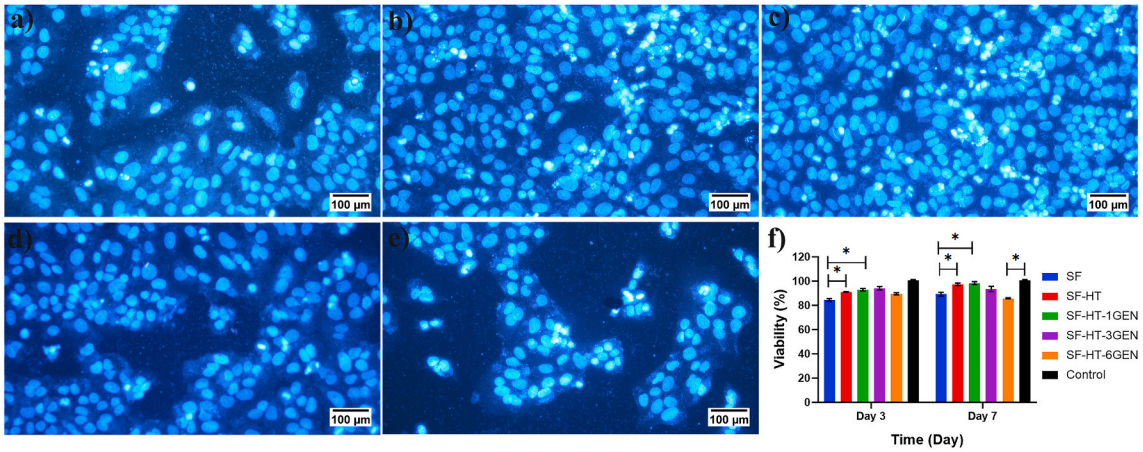

Fig. 5. In vitro cell study. Cell coverage on scaffold for (a) SF, (b) SF-HT, (c) SF-HT-1GEN, (d) SF-HT-3GEN, and (e) SF-HT-6GEN. (f) Indirect MTT assay of different scaffold material compositions over 7 days of culture (*p < 0.05, Control = well plates without scaffolds).

fixed scaffolds at 2 and 4 weeks, post-implantation (Fig. 6a and b). It was observed that the scaffold maintained its general shape throughout the implantation (Fig. 6a) and integrated with the host tissue. By week 2, the dermis tissue surrounding the implant displayed symptoms of a mild to moderate immune response. Further, fibrous connective tissue is detectable in the H&E staining result at week 2. The number of inflammatory cells close to the remnant scaffold margin is higher than in other areas of fibrous connective tissue (Fig. 6b). These inflammatory cells are mainly foreign body giant cells (FBGCs), macrophages, and lymphocytes. Fibrous tissue in the areas far from the remnant scaffold margin was composed of abundant active fibroblasts, newly formed vessels, and showed mild to moderate infiltration of mononuclear inflammatory cells. Collagen deposition was initiated by week 2, however the main components of this connective tissue were cells. By week 4, we observed significantly more collagen fibers and newly formed vessels compared to week 2, in addition to decreased cellularity. Multiple studies have shown that SF and HT work to enhance *in vivo* vascularization [56,57], and Wang et al. demonstrated that HT-loaded implants promoted both osteogenesis and angiogenesis in calvarial defects after 4 weeks [57]. Therefore, we conclude that the neovascularization demonstrated in this *in vivo* study was induced by the scaffold material composition of SF and HT.

5. Conclusions

This work reports on the fabrication, *in vitro*, and *in vivo* characterization of GEN-loaded HF-SF nanofibrous scaffolds for bone tissue engineering applications. The presence of HT in the scaffolds improved cell attachment and proliferation in osteoblast cell lines. Sustained release of GEN from the scaffolds was achieved via encapsulation of the drug during the electrospinning process, for a period greater than 7 days. Increasing the concentration of the loaded antibiotic resulted in higher antibacterial activity of the scaffolds, however high antibiotic loading (6%wt) causes cell toxicity in osteoblasts. The observed results proved the occurrence of antibiotic loading within the nanofibers. The bioactivity of the loaded GEN was evaluated by performing a disc diffusion assay for *E. coli* and *S. aureus*, with the results confirming that the manufacturing process did not have an adverse effect on the activity of the drug. The *in vivo* results showed that subcutaneous implantation of SF-HT-3GEN scaffolds did not induce a severe inflammatory response in rodents, after 4 weeks of implantation. Finally, the *in vivo* vascularization induced by the implanted SF-HT-3GEN composite scaffolds indicates an additional benefit of this composite scaffold for bone tissue engineering applications. These results suggest that the GEN-loaded HF-SF scaffolds may have specific applications as bone scaffold materials, in addition to broader tissue engineering applications.

Funding

This work was supported by the Canadian Institutes of Health Researches, Natural Sciences and Engineering Research Council of Canada (NSERC), Canada Foundation for Innovation (CFI), and 4 M Biotech Inc.

CRediT authorship contribution statement

Zhina Hadisi: Methodology, Investigation, Writing - original draft, Formal analysis. **Hamid Reza Bakhsheshi-Rad:** Investigation, Writing - review & editing. **Tavia Walsh:** Writing - review & editing. **Mohammad Mehdi Dehghan:** Writing - original draft, Writing - review & editing. **Saeed Farzad-Mohajeri:** Writing - original draft. **Hossein Gholami:** Methodology. **Anahita Diyanoush:** Writing - original draft. **Erik Pagan:** Visualization. **Mohsen Akbari:** Conceptualization, Supervision, Funding acquisition.

Declaration of competing interest

The authors declare that they have no known competing financial interests or personal relationships that could have appeared to influence

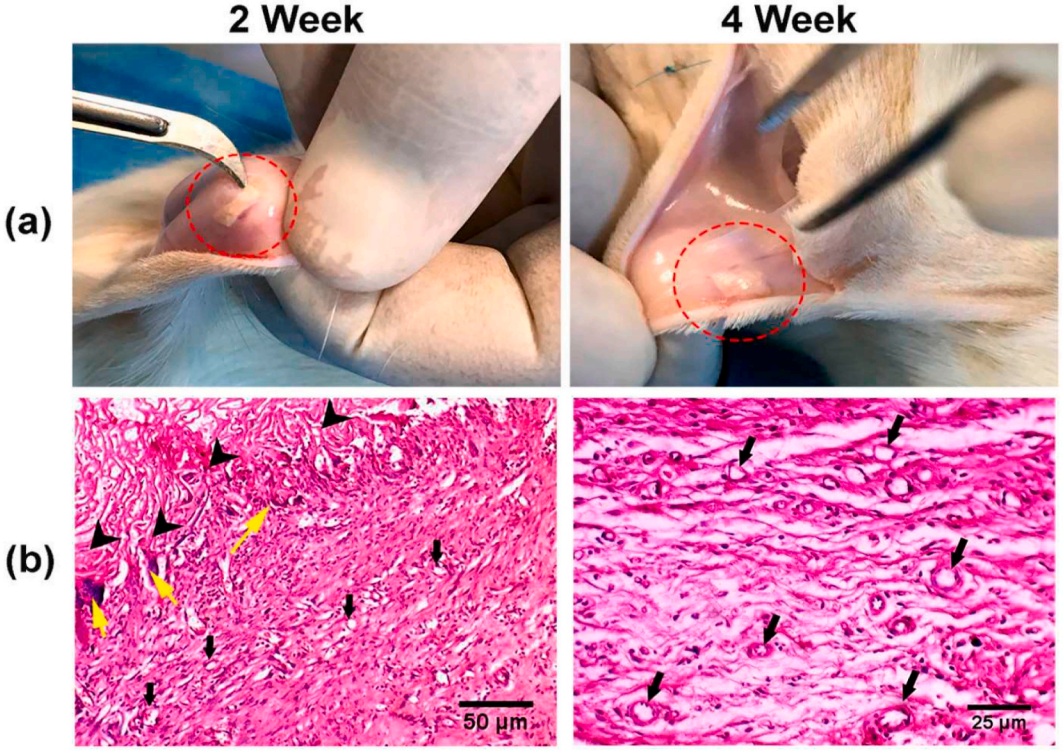

Fig. 6. Subcutaneous scaffold implantation. (a) Macroscopic images from subcutaneous implantation of SF-HT-3GEN scaffolds for 2 weeks and 4 weeks, respectively (red circles show the implanted scaffold). (b) Tissue sections with H&E staining (black arrowheads point to the remnant scaffold margin, black arrows to the newly-formed blood vessels, and yellow arrows to the FBGCs).

the work reported in this paper.

Appendix A. Supplementary data

Supplementary data to this article can be found online at https://doi.org/10.1016/j.polymertesting.2020.106698.

References

[1] R. Raggio, et al., Silk fibroin porous scaffolds loaded with a slow-releasing hydrogen sulfide agent (GYY4137) for applications of tissue engineering, ACS Biomater. Sci. Eng. v4 (2018) 2956–2966.
[2] D. Yao, et al., Salt-leached silk scaffolds with tunable mechanical properties, Biomacromolecules v13 (2012) 3723–3729.
[3] B. Sarker, W. Li, K. Zheng, R. Detsch, A.R. Boccaccini, Designing porous bone tissue engineering scaffolds with enhanced mechanical properties from composite hydrogels composed of modified alginate, gelatin, and bioactive glass, ACS Biomater. Sci. Eng. v2 (2016) 2240–2254.
[4] H. Maleki, et al., Mechanically strong silica-silk fibroin bioaerogel: a hybrid scaffold with ordered honeycomb micromorphology and multiscale porosity for bone regeneration, ACS Appl. Mater. Interfaces 11 (19) (2019) 17256–17269, https://doi.org/10.1021/acsami.9b04283.
[5] R.J. Jackson, et al., Chemically treated 3D printed polymer scaffolds for biomineral formation, ACS Omega v3 (2018) 4342–4351.
[6] V.L. Tsang, S.N. Bhatia, "Fabrication of three-dimensional tissues," in tissue engineering II, in: K. Lee, D. Kaplan (Eds.), Advances In Biochemical Engineering/Biotechnology, V103, Springer, Berlin, Heidelberg, 2005, pp. 189–205.
[7] B. Huang, G. Caetano, C. Vyas, J. Blaker, C. Diver, P. Bártolo, Polymer-ceramic composite scaffolds: the effect of hydroxyapatite and β-tri-calcium phosphate, Materials v11 (2018) 129.
[8] M. Tahriri, et al., Evaluation of the in vitro biodegradation and biological behavior of poly(lactic-co-glycolic acid)/nano-fluorhydroxyapatite composite microsphere-sintered scaffold for bone tissue engineering, J. Bioact. Compat Polym. v33 (2018) 146–159 (in English).
[9] B. Huang, P.J. Bártolo, Rheological characterization of polymer/ceramic blends for 3D printing of bone scaffolds, Polym. Test. v68 (2018) 365–378.
[10] S. Mohammadi, et al., Fabrication of nanofibrous PVA/Alginate-Sulfate substrates for growth factor delivery, J. Biomed. Mater. Res. v107 (2019) 403–413.
[11] D.X. Chen, Extrusion Bioprinting of Scaffolds for Tissue Engineering Applications, vol. XI, Springer International Publishing, 2018, p. 171.
[12] N.G. Sahoo, Y.Z. Pan, L. Li, C.B. He, Nanocomposites for bone tissue regeneration, Nanomedicine v8 (2013) 639–653.
[13] D.J. Barone, J.M. Raquez, P. Dubois, Bone-guided regeneration: from inert biomaterials to bioactive polymer (nano) composites, Polym. Adv. Technol. v22 (2011) 463–475.
[14] F. Sun, H. Zhou, J. Lee, Various preparation methods of highly porous hydroxyapatite/polymer nanoscale biocomposites for bone regeneration, Acta Biomater. v7 (2011) 3813–3828.
[15] J. Huang, et al., In vitro assessment of the biological response to nano-sized hydroxyapatite, J. Mater. Sci. Mater. Med. v15 (2004) 441–445.
[16] P.V. Gnaneshwar, et al., Ramification of zinc oxide doped hydroxyapatite biocomposites for the mineralization of osteoblasts, Mater. Sci. Eng. C v96 (2019) 337–346.
[17] J. Lu, et al., The biodegradation mechanism of calcium phosphate biomaterials in bone, J. Biomed. Mater. Res. v63 (2002) 408–412.
[18] H. Ma, C. Feng, J. Chang, C. Wu, 3D-printed bioceramic scaffolds: from bone tissue engineering to tumor therapy, Acta Biomater. 79 (2018) 37–59, https://doi.org/10.1016/j.actbio.2018.08.026.
[19] H. Mohammadi, et al., Bioinorganics in bioactive calcium silicate ceramics for bone tissue repair: bioactivity and biological properties, J. Ceram. Sci. Technol. v5 (2014) 1–12.
[20] M. Shi, et al., Stimulation of osteogenesis and angiogenesis of hBMSCs by delivering Si ions and functional drug from mesoporous silica nanospheres, Acta Biomater. v21 (2015) 178–189.
[21] L.-C. Gerhardt, et al., The pro-angiogenic properties of multi-functional bioactive glass composite scaffolds, Biomaterials v32 (2011) 4096–4108.
[22] A.K. Jaiswal, H. Chhabra, S.S. Kadam, K. Londhe, V.P. Soni, J.R. Bellare, Hardystonite improves biocompatibility and strength of electrospun polycaprolactone nanofibers over hydroxyapatite: a comparative study, Mater. Sci. Eng. C v33 (2013) 2926–2936.
[23] B. Dhandayuthapani, Y. Yoshida, T. Maekawa, D.S. Kumar, Polymeric scaffolds in tissue engineering application: a review, Int. J. Polym. Sci. (2011) 2011, v.
[24] M.I. Sabir, X. Xu, L. Li, A review on biodegradable polymeric materials for bone tissue engineering applications, J. Mater. Sci. v44 (2009) 5713–5724.
[25] Y. Gao, Y. Wang, Y. Wang, W. Cui, Fabrication of gelatin-based electrospun composite fibers for anti-bacterial properties and protein adsorption, Mar. Drugs v14 (2016).
[26] S. Babitha, et al., Fabrication of a biomimetic ZeinPDA nanofibrous scaffold impregnated with BMP-2 peptide conjugated TiO 2 nanoparticle for bone tissue engineering, J. Tissue Eng. Regen. Med. v12 (2018) 991–1001.
[27] M. Kouhi, V.J. Reddy, M. Fathi, M. Shamanian, A. Valipoouri, S. Ramakrishna, Poly (3-hydroxybutyrate-co-3-hydroxyvalerate)/fibrinogen/bredigite nanofibrous membranes and their integration with osteoblasts for guided bone regeneration, J. Biomed. Mater. Res. v107 (2019).
[28] G. BaoLin, P.X. Ma, Synthetic biodegradable functional polymers for tissue engineering: a brief review, Sci. China Chem. v57 (2014) 490–500.
[29] J. Melke, S. Midha, S. Ghosh, K. Ito, S. Hofmann, Silk fibroin as biomaterial for bone tissue engineering, Acta Biomater. v31 (2016) 1–16.
[30] J.-Y. Kim, B.-E. Yang, J.-H. Ahn, S.O. Park, H.-W. Shim, Comparable efficacy of silk fibroin with the collagen membranes for guided bone regeneration in rat calvarial defects, J. Adv. Prosthodont v6 (2014) 539–546.
[31] K.-H. Kim, et al., Biological efficacy of silk fibroin nanofiber membranes for guided bone regeneration, J. Biotechnol. v120 (2005) 327–339.
[32] V. Mouriño, J.P. Cattalini, J.A. Roether, P. Dubey, I. Roy, A.R. Boccaccini, Composite polymer-bioceramic scaffolds with drug delivery capability for bone tissue engineering, Expet Opin. Drug Deliv. v10 (2013) 1353–1365.
[33] J. Pant, J. Sundaram, M.J. Goudie, D.T. Nguyen, H. Handa, Antibacterial 3D bone scaffolds for tissue engineering application, J. Biomed. Mater. Res. B v107 (2019) 1068–1078.
[34] E. Sarigol-Calamak, C. Hascicek, Tissue scaffolds as a local drug delivery system for bone regeneration, in: Cutting-Edge Enabling Technologies for Regenerative Medicine, Springer, Singapore, 2018, pp. 475–493.
[35] P. Pankongadisak, N. Jaikaew, K. Kiti, B. Chuenjitkuntaworn, P. Supaphol, O. Suwantong, The potential use of gentamicin sulfate-loaded poly (l-lactic acid)-sericin hybrid scaffolds for bone tissue engineering, Polym. Bull. (2018) 1–19.
[36] Z. Hadisi, J. Nourmohammadi, J. Mohammadi, Composite of porous starch-silk fibroin nanofiber-calcium phosphate for bone regeneration, Ceram. Int. v41 (2015) 10745–10754.
[37] A. Sionkowska, B. Kaczmarek, R. Gadzala-Kopciuch, Gentamicin release from chitosan and collagen composites, J. Drug Deliv. Sci. Technol. v35 (2016) 353–359.
[38] Z. Hadisi, J. Nourmohammadi, S.M. Nassiri, The antibacterial and anti-inflammatory investigation of Lawsonia Inermis-gelatin-starch nano-fibrous dressing in burn wound, Int. J. Biol. Macromol. v107 (2018) 2008–2019.
[39] H. Bakhsheshi-Rad, Z. Hadisi, E. Hamzah, A. Ismail, M. Aziz, M. Kashefian, Drug delivery and cytocompatibility of ciprofloxacin loaded gelatin nanofibers-coated Mg alloy, Mater. Lett. v207 (2017) 179–182.
[40] Y. Zhou, H. Yao, J. Wang, D. Wang, Q. Liu, Z. Li, Greener synthesis of electrospun collagen/hydroxyapatite composite fibers with an excellent microstructure for bone tissue engineering, Int. J. Nanomed. v10 (2015) 3203.
[41] D. Reffitt, et al., Orthosilicic acid stimulates collagen type 1 synthesis and osteoblastic differentiation in human osteoblast-like cells in vitro, Bone v32 (2003) 127–135.
[42] A.K. Gaharwar, et al., Bioactive silicate nanoplatelets for osteogenic differentiation of human mesenchymal stem cells, Adv. Mater. v25 (2013) 3329–3336.
[43] W. Wang, et al., Development of novel implants with self-antibacterial performance through in-situ growth of 1D ZnO nanowire, Colloids Surf. B Biointerfaces v141 (2016) 623–633.
[44] J.R. Popp, B.J. Love, A.S. Goldstein, Effect of soluble zinc on differentiation of osteoprogenitor cells, J. Biomed. Mater. Res. v81 (2007) 766–769.
[45] J. Jeong, J.H. Kim, J.H. Shim, N.S. Hwang, C.Y. Heo, Bioactive calcium phosphate materials and applications in bone regeneration, Biomater. Res. v23 (2019) 4.
[46] M.M. Dvorak, et al., Physiological changes in extracellular calcium concentration directly control osteoblast function in the absence of calciotropic hormones, Proc. Natl. Acad. Sci. U. S. A. v101 (2004) 5140–5145.
[47] C.T. Johnson, A.J. García, Scaffold-based anti-infection strategies in bone repair, Ann. Biomed. Eng. v43 (2015) 515–528.
[48] Y. Chang, C. Tai, P. Hsieh, S. Ueng, Gentamicin in bone cement: a potentially more effective prophylactic measure of infection in joint arthroplasty, Bone Joint Res. v2 (2013) 220–226.
[49] M.L. Azi, M. Kfuri Junior, R. Martinez, C.A.J. Paccola, Bone cement and gentamicin in the treatment of bone infection: background and in vitro study, Acta Ortopédica Bras. v18 (2010) 31–34.
[50] A.I. Barzic, S. Ioan, Antibacterial Drugs—From Basic Concepts to Complex Therapeutic Mechanisms of Polymer Systems, Oncepts, Compounds and the Alternatives of Antibacterials, IntechOpen, 2015.
[51] R.N. Granito, A.C.M. Renno, H. Yamamura, M.C. de Almeida, P.L.M. Ruiz, D. A. Ribeiro, Hydroxyapatite from fish for bone tissue engineering: a promising approach, Int. J. Mol. Cell Med. v7 (2018) 80.
[52] H. Bakhsheshi-Rad, et al., Novel nanostructured baghdadite-vancomycin scaffolds: *in-vitro* drug release, antibacterial activity and biocompatibility, Mater. Lett. v209 (2017) 369–372.
[53] M. Parent, et al., Hydroxyapatite microporous bioceramics as vancomycin reservoir: antibacterial efficiency and biocompatibility investigation, J. Biomater. Appl. v31 (2016) 488–498.
[54] ISO 10993-1:2018, FDA-2013-D-0350, 2018.
[55] S. Gogolewski, Bioresorbable polymers in trauma and bone surgery, Injury v31 (2000) D28–D32.
[56] H. Han, et al., Silk biomaterials with vascularization capacity, Adv. Funct. Mater. v26 (2016) 421–432.
[57] G. Wang, et al., Effects of Sr-HT-Gahnite on osteogenesis and angiogenesis by adipose derived stem cells for critical-sized calvarial defect repair, Sci. Rep. v7 (2017) 41135.